Available online at www.sciencedirect.com
SCIENCE DIRECT®
Journal of Computational Physics 209 (2005) 559–581
JOURNAL OF COMPUTATIONAL PHYSICS
www.elsevier.com/locate/jcp

Using semiclassical trajectories for the time-evolution of interacting quantum-mechanical systems

D.E. Dauger [a,b,*], V.K. Decyk [b], J.M. Dawson [b,1]

[a] *Dauger Research, Inc., P.O. Box 3074, Huntington Beach, CA 92605, USA*
[b] *UCLA Plasma Physics Group, Department of Physics and Astronomy, University of California, Los Angeles, CA 90095, USA*

Received 9 September 2004; received in revised form 10 February 2005; accepted 9 March 2005
Available online 23 May 2005

Abstract

We have developed a method that recasts the time-propagation of dynamic, mutually interacting quantum-mechanical wavefunctions principally as the time-evolution of many classical particles. Our approach utilizes an approximation of Feynman path integrals, known as the semiclassical method, to reduce the path integral to only the ''classical'' paths connecting the wavefunction at one time step to the next. In exchange for simplifying the path sampling, each classical path's contribution gains a determinant term dependent on the path and its environment. Like virtual particles in quantum field theory, ''virtual classical particles'' are said to follow these classical paths. Pushing these virtual classical particles provides the necessary data to evolve quantum wavefunctions in time. Particle-based techniques implemented on parallel computers can then be used to propagate quantum systems using this alternative method.

MSC: 81-08; 81S40; 81Q20; 81Q30; 81Q05; 81Q99; 65-04; 65Z05; 65C35; 65P99; 37M05; 68U20; 68W10

Keywords: Quantum particle-in-cell; Semiclassical; Path integral; Time evolving; Interacting; Stationary phase; Parallel computation; Plasma PIC; Feynman; Particle-based; WKB; Lagrangian; Grid method

1. Introduction

1.1. Motivation

Microscopic behavior of multiparticle quantum systems is among the most difficult problems to study. A variety of important physical systems, from the interior of the sun to protein folding and quantum

* Corresponding author. Tel.: +1 714 840 0013; fax: +1 714 840 0224.
E-mail address: d@daugerresearch.com (D.E. Dauger).
[1] Deceased.

0021-9991/$ - see front matter © 2005 Elsevier Inc. All rights reserved.
doi:10.1016/j.jcp.2005.03.028

chemistry to metals and semiconductor surfaces, are explained only by incorporating the quantum effects these particles exhibit.

Incorporating quantum effects into the model can be important when the best fidelity to the physics is required, but addressing quantum phenomena correctly and efficiently is usually nontrivial. Various methods that address multiparticle quantum behavior exist, varying in complexity and accuracy. Among the candidates are mean-field methods and their extensions applied to solutions determined using the Schrödinger equation, usually using a finite-difference or spectral method [1–3]. Other methods exist that approximate the particles as Gaussian wavepackets. Some use a "frozen" Gaussians, i.e., those of fixed width [4], to evolve a wavefunction, while others use Gaussians with parameters that change in response to the system [5].

1.2. Background of the approach

Our approach is to use a large number of classical paths to compute the evolution of quantum wavefunctions. This idea originated in the birth of quantum mechanics. De Broglie was first to suggest, in his 1924 thesis [6], that matter has wave properties. He proposed that a particle of matter, like light, gains phase as it travels. Inspired by the similarity between Fermat's principle and the principle of least action, he identified matter's phase with *the classical action*, the integral of the Lagrangian, *along the particle's path*. Reinterpreting Planck's concept of the *quanta* and Einstein's light quantization rule instead for matter, he applied this idea to create a model of the atom that quantitatively and conceptually explained Bohr's earlier atomic model. De Broglie's model predicted that electrons will only be stable in particular orbits around a nucleus because the electron's phase constructively interferes, resonating like a standing wave, on the orbit's *path*. The rules governing this behavior of light and matter came to be known as *quantum mechanics*.

In 1928, Van Vleck [7] generalized the WKB method [8], which was developed in 1926 to help find approximate solutions to Schrödinger's equation [9], to higher dimensions and derived the appearance of the classical action in a complex exponential, to be later identified as a propagator. This work was among the earliest to show connections between classical mechanics and quantum mechanics.

Inspired by discoveries of Dirac [10], Feynman published his seminal paper [11] on path integrals in 1948. The evolution of a particle could be modeled as a sum over possible paths whose contributions are described by a propagator. This paper was significant because it demonstrated explicitly how Feynman's rigorous form of path integration can be used to derive quantum mechanics, clearly establishing the technique's relevance as a method alternative to that of Schrödinger while being a more direct application and generalization of de Broglie's original idea. Also based on Dirac's work, he showed how, in typical cases, a sum over these paths through space could be seen to simplify to a sum of classical paths. The familiar arising from the unfamiliar, classical dynamics was seen to arise out of a purely quantum-mechanical concept, providing a clear connection between classical and quantum theory. The term *semiclassical* was later coined for this apparent merge of classical and quantum ideas.

Feynman later built on his path integral work [12]. In 1967, Gutzwiller [13] used Feynman's path integrals to rederive Van Vleck's propagator with the addition of phase corrections due to caustics along periodic orbits. These caustics were identified by properties of the eigenvalues of the semiclassical matrix, used in the determinant factor that expresses focusing in the application of the WKB-like methods to semiclassical paths.

In the early 1990s, Heller and Tomsovic produced a series of articles [14–18] demonstrating accuracy and stability of quantum-mechanical calculations using long classical paths based on the formula of Van Vleck, Maslov [19], and Gutzwiller. Some of the techniques built upon the developments of many others [20]. These and related work [21,22] provided evidence, at least for single particle cases, for the computational viability of using many classical paths to answer specific questions about quantum-mechanical systems, including those that are chaotic.

Meanwhile, plasma physics developed significantly in the last half of the 20th century. Plasmas, by definition, are collections of particles under the influence of their mutual electromagnetic fields and following paths determined by classical mechanics. Buneman and Dawson [23–26] developed the earliest computational models of plasmas. These systems were one-dimensional "sheet models" of the plasma, and efficient computational techniques for such models were developed [27]. Later, these models were extended to two and three dimensions by introducing methods to efficiently solve for electrostatic fields and combining the use of grid points [28] with the application of a Fast Fourier Transform (FFT) algorithm [29] to solving Poisson's equation in Fourier space [30]. These developments made efficient modeling of multidimensional plasmas possible.

Further improvements in plasma modeling came in step with the evolution of computational hardware. In particular, Particle-In-Cell (PIC) techniques to model plasmas on parallel computing hardware has seen great strides in work by Dawson, Decyk, and others [30–36]. Such plasma PIC simulations effectively and efficiently utilize such computational resources, achieving 90% parallelism and 40% of estimated peak hardware speed. In the 1990s, problems involving up to 2×10^8 particles on 32×10^6 grid points in three dimensions have become possible. These methods are shown to be robust and portable [37,38], and have run successfully on a wide range of computers (e.g., Cray-90s, T3Ds, T3Es, SGIs, IBM SP2s, and Macintosh clusters [39]).

Dawson, familiar with the efficiency of these plasma methods to manage particles and calculate their classical paths, conceived of the idea to apply these techniques to the classical paths in the semiclassical methods referred to by Heller and Tomsovic [16]. If we assume thousands of classical paths could be used to evolve a system of one quantum particle, then could millions of classical paths be used to evolve a system of hundreds, or perhaps thousands, of quantum particles?

If successful, such a code could model scores of phenomena where quantum effects are important and answer some of the most difficult questions involving quantum mechanics. This modeling method would allow a detailed investigation of optical properties, ionization potential, conductance, and a host of other experimentally determined material properties. This tool could be used for the design and physical understanding of devices where quantum mechanics is important. Ultimately, with the incorporation of multiple dimensions, spin phenomena, and electromagnetism, this method would be able to model atoms, chemical reactions, quantum electronics, solid-state physics, and a multitude of other addressable physical problems. Cross-pollinated from plasma computation and semiclassical and quantum theory, this idea and its potential implications are the motivation of this work.

1.3. Other applications of semiclassical methods

Many applications of semiclassical methods and their derivatives have been accomplished. These are usually directed at particular properties of a quantum system, most commonly the energy spectrum, using a wide variety of approaches [14,16,18,20,22,40–48]. Some have met with great success, and some are limited in quality for long time scales. The authors find the reference by Schulman [20] to continue to be an excellent authority on path integration, while other references [49] reflect more recent work.

Computational application of semiclassical methods most commonly use the Van Vleck–Gutzwiller–Maslov propagator. For example, based on work by Heller [50], Simotti et al. [51] have developed clever methods for solving for time-independent eigenstates of two-dimensional billiard-type quantum systems. They focus on constructing the eigenstate data at the boundary of the system using a superposition of plane waves determined by segments of periodic classical orbits they locate in the system. Their methods use the Van Vleck–Gutzwiller–Maslov propagator to determine relevant properties of these periodic orbits. They then use Green's theorem to derive the interior of the eigenstate using the boundary information. Other work on time-dependent propagation of wavefunctions using classical paths and that propagator are rare and meet with limited success [14].

The work presented in this article is directly uses classical paths to accurately propagate time-dependent quantum wavefunctions in a way that diverges from previous work. In this work, we derive a propagator directly from basic quantum mechanics and Feynman path integrals. This propagator is designed for the computational time-dependent evolution of dynamic discretized wavefunctions. Its derivation is guided by the form of the Van Vleck propagator, Gutzwiller's work, and a section of Chapter 14 of [20]. Otherwise, this computational method, its development, implementation, study, and application are new and not found in previous published literature.

This article presents a new way to apply semiclassical methods designed for interacting particles represented as quantum wavefunctions. Our approach explicitly traces classical paths over time intervals that are short by comparison to most other uses of semiclassical methods in previous literature. The method in the article then processes data collected on those paths to fully reconstruct the new wavefunction at a later time step. New classical paths are created from that new wavefunction. This approach gives us two features of great interest to us: (1) It allows the environment around the wavefunction to change in a short period of time. That opens an obvious mechanism for interactions from other wavefunctions or changing conditions of the system, particularly, a time-dependent effective potential. (2) Issues raised by undesirable behaviors of the semiclassical determinant, such as singularities, do not affect this method. That feature, made possible by the short paths, obviates the need for a Maslov factor or more complex analyses of the system, easing the implementation of this approach.

We are exploring a different problem space than what has typically been performed with semiclassical methods. As a result, this use of semiclassical methods makes certain computational and physical scenarios possible to explore. We make use of (comparatively) "short" classical paths in a semiclassical context. With this approach, the form of the calculation becomes amenable to implementation on massively parallel computers using techniques originally developed for classical plasma simulations.

This article is an exposition of methods used to combine the semiclassical methods for solving quantum-mechanical problems with computational techniques from plasma PIC simulations for implementation on parallel computers. It is meant to serve as a guide for future use and development of both the existing quantum PIC code and any future codes using similar techniques. The body of this article provides a theoretical foundation for such approaches to modeling quantum-mechanical wavefunctions.

1.4. Conventions

The convention used in this presentation uses the Dirac bra-ket notation ($|\psi\rangle$) to represent wavefunctions. The position operator $\hat{x}$ has an associated complete position basis set $\{|x\rangle\}$, and its dual is the momentum operator $\hat{p}$ with its complete momentum basis set $\{|p\rangle\}$. These spaces are related through the Fourier transform kernel, $\langle x|p\rangle = \frac{1}{\sqrt{h}} \exp\left(\frac{2\pi i x p}{h}\right)$, where h is Planck's constant. The time-dependent Schrödinger equation is $\hat{H}|\psi\rangle = i\hbar \frac{\partial}{\partial t}|\psi\rangle$, where $\hat{H}$ is the Hamiltonian operator and $\hbar \equiv h/2\pi$. This convention is best expressed in a reference by Townsend [52].

2. Theory

2.1. The approach

To evolve a set of quantum-mechanical wavefunctions, our approach is the following: Each wavefunction can be evolved using a large number of arbitrary paths. Because of the nature of the contributions of these paths, the total contribution can be simplified to just those from the classical paths. These

contributions form the wavefunction at the new time step. Duplicating this procedure for all wavefunctions updates the entire system to the new time step, allowing the process to repeat.

We begin with the paths used for Feynman path integrals [11]. More commonly used in quantum field theory, these paths begin at an initial position in the wavefunction at the earlier time step, weave their way through space, and end at a final position in the wavefunction at the later time step. The contribution of this path is the wavefunction evaluated at the beginning of the path multiplied by a complex number whose phase is proportional to the action, the integral of the Lagrangian, along that path. These contributions are summed to form the new wavefunction.

The technique used to simplify the contributions to the classical paths is called a "semiclassical approximation". Although not exactly identical, it has much in common with WKB techniques and stationary-phase methods. It involves summing the contributions from paths with the same initial and final positions. The result is that the paths in the vicinity of the path whose action is an extremum provide the most significant contributions. The property of these paths the reader should focus on is their phase. The phase difference between paths changes as a function of their variation off the extremum path. In part because Planck's constant is so small, it tends to be the case that this phase difference increases quickly with variation. This property is essential to this approximation. Its key is in showing that this rapid variation in phase causes their contributions to cancel each other. This cancellation dominates over all other effects. The special path with the extremum action, also found using the Lagrangian-based calculus of variations of classical mechanics, is called the classical path.

In the following sections, we will show derivations of the semiclassical methods, from their start in basic quantum mechanics to the complete contributions of the classical paths given by the semiclassical approximation. We show these derivations because of two problems found in the course of this work: (1) Other than this article, such calculations could not be found together in detail in any other source. (2) Previous results (such as the Van Vleck–Gutzwiller–Maslov [22] propagator) were found to be inappropriate to this application. To overcome these difficulties, the authors reconstructed the semiclassical derivations from basic quantum theory and customized them for this application. In the context of quantum field theory, *virtual particles* are said to follow the paths forming a Feynman path integral. Likewise, we coin the term "*virtual classical particles*", which trace the classical paths in this discussion.

2.2. Feynman path integrals

The theoretical basis for the quantum-mechanical methods used here is the Feynman path integral. We begin with a result of the time-dependent Schrödinger equation, which will allow us to derive a precise Feynman path integral more quickly. Consider the time evolution of one wavefunction, $|\psi\rangle$, over an interval from t to $t + \Delta t$,

$$|\psi(t+\Delta t)\rangle = \exp\left(-\frac{\mathrm{i}\hat{H}\Delta t}{\hbar}\right)|\psi(t)\rangle, \tag{1}$$

where $\hbar$ is Planck's constant divided by 2π, and $\hat{H}$ is the complete Hamiltonian,

$$\hat{H} = \sum_l \frac{\hat{p}_l^2}{2m} + \sum_l V_l(\hat{x}_l), \tag{2}$$

where V_l is the effective potential encountered by particle l. Define $|\psi_f\rangle \equiv |\psi(t+\Delta t)\rangle$ and $|\psi_0\rangle \equiv |\psi(t)\rangle$. We then divide this time interval into N intervals, each spaced by ∂t_i for $0 \leqslant i \leqslant N$ where

$$\sum_{i=1}^{N} \partial t_i = \Delta t \quad \text{and} \quad \partial t_i > 0 \qquad \forall i. \tag{3}$$

Inserting

$$\mathbf{1} = \int |x\rangle \langle x| \, \mathrm{d}x, \tag{4}$$

(1) becomes

$$|\psi_f\rangle = \int \prod_{j=0}^{N} \mathrm{d}x_j \, |x_N\rangle \langle x_N| \exp\left(-\frac{\mathrm{i}\hat{H}\partial t_N}{\hbar}\right) |x_{N-1}\rangle \cdots \langle x_i| \exp\left(-\frac{\mathrm{i}\hat{H}\partial t_i}{\hbar}\right) |x_{i-1}\rangle \cdots \langle x_1| \exp\left(-\frac{\mathrm{i}\hat{H}\partial t_i}{\hbar}\right) |x_0\rangle \langle x_0|\psi_0\rangle, \tag{5}$$

an $N+1$-dimensional integral. Considering the ith term, we insert

$$\mathbf{1} = \int |p_i\rangle \langle p_i| \, \mathrm{d}p_i \tag{6}$$

and obtain

$$\langle x_i| \exp\left(-\frac{\mathrm{i}\hat{H}\partial t_i}{\hbar}\right) |x_{i-1}\rangle = \int \mathrm{d}p_i \, \langle x_i| \exp\left(-\frac{\mathrm{i}\hat{H}\partial t_i}{\hbar}\right) |p_i\rangle \langle p_i|x_{i-1}\rangle. \tag{7}$$

After assuming ∂t_i is small, substitute the Hamiltonian, and multiply through

$$\langle x_i| \exp\left(-\frac{\mathrm{i}\hat{H}\partial t_i}{\hbar}\right) |p_i\rangle \approx \langle x_i|p_i\rangle - \frac{\mathrm{i}\partial t_i}{\hbar}\left(\langle x_i| \frac{\hat{p}^2}{2m} |p_i\rangle + \langle x_i|V(\hat{x})|p_i\rangle\right). \tag{8}$$

After hitting the kinetic energy term on the momentum ket and the potential energy term on the position ket, we can reconstitute and factor the exponential

$$\langle x_i| \exp\left(-\frac{\mathrm{i}\hat{H}\partial t_i}{\hbar}\right) |p_i\rangle \approx \langle x_i|p_i\rangle \exp\left(-\frac{\mathrm{i}\partial t_i}{\hbar}\left(\frac{p_i^2}{2m} + V(x_i)\right)\right). \tag{9}$$

Using (9) and $\langle x|p\rangle = \frac{1}{\sqrt{h}} \exp(\mathrm{i}xp/\hbar)$, the integrand of (7) becomes

$$\langle x_i|p_i\rangle \exp\left(-\frac{\mathrm{i}\partial t_i}{\hbar}\left(\frac{p_i^2}{2m} + V(x_i)\right)\right) \langle p_i|x_{i-1}\rangle = \frac{1}{h} \exp\left(\frac{\mathrm{i}p_i(x_i - x_{i-1})}{\hbar} - \frac{\mathrm{i}\partial t_i}{\hbar}\left(\frac{p_i^2}{2m} + V(x_i)\right)\right). \tag{10}$$

We define $\dot{x}_i \equiv \frac{x_i - x_{i-1}}{\partial t_i}$, substitute, factor, and completing the square gives

$$\begin{aligned} \langle x_i| \exp\left(-\frac{\mathrm{i}\hat{H}\partial t_i}{\hbar}\right) |x_{i-1}\rangle &\approx \int \mathrm{d}p_i \frac{1}{h} \exp\left(-\frac{\mathrm{i}\partial t_i}{\hbar}\left(\frac{(p_i - m\dot{x}_i)^2}{2m} - \frac{m\dot{x}_i^2}{2} + V(x_i)\right)\right) \\ &= \exp\left(\frac{\mathrm{i}\partial t_i}{\hbar}\left(\frac{m\dot{x}_i^2}{2} - V(x_i)\right)\right) \int \mathrm{d}p_i \frac{1}{h} \exp\left(-\frac{\mathrm{i}\partial t_i}{\hbar} \frac{(p_i - m\dot{x}_i)^2}{2m}\right). \end{aligned} \tag{11}$$

We recognize that this is a Gaussian integral with a complex exponential, so we use a convergence factor. Also, if we define $L(x_i, \dot{x}_i) \equiv \frac{m\dot{x}_i^2}{2} - V(x_i)$, then

$$\langle x_i| \exp\left(-\frac{\mathrm{i}\hat{H}\partial t_i}{\hbar}\right) |x_{i-1}\rangle \approx \exp\left(\frac{\mathrm{i}\partial t_i}{\hbar} L(\dot{x}_i, x_i)\right) \sqrt{\frac{\mathrm{im}}{h\partial t}}. \tag{12}$$

Note that we recognize $L(x_i, \dot{x}_i)$ as the Lagrangian. We obtain

$$|\psi_f\rangle = \int \prod_{j=0}^{N} \mathrm{d}x_j \, |x_N\rangle \left(\frac{\mathrm{im}}{h\partial t}\right)^{N/2} \exp\left(\frac{\mathrm{i}}{\hbar} \sum_{i=1}^{N} L(x_i, \dot{x}_i)\partial t_i\right) \langle x_0|\psi_0\rangle, \tag{13}$$

which is the path integral from $|\psi_0\rangle$ to $|\psi_f\rangle$ using discrete time steps. In some notations [12], a $\mathscr{D}$ is used for the product of differentials. (13) is called a Feynman path integral. (The above derivation is largely similar to one in Chapter 8 of [52].)

Note that the sum inside the exponential is a time integral of the Lagrangian on a path described by $\{x_i\}$ (which uniquely determine $\{\dot{x}_i\}$). This sum is the action S along this path:

$$S \equiv \sum_{i=1}^{N} L(x_i, \dot{x}_i)\partial t_i. \tag{14}$$

These paths are diagrammatically shown in Fig. 1.

Note that, at this point, other than the modest requirements used so far, the paths are arbitrary and unrestricted. The particles that follow these paths are called *virtual particles*.

2.3. The semiclassical approximation

We now consider variations $\{\partial x_i\}$ from a special path we label $\{x_{cl_i}\}$, where $1 \leqslant i < N$. Further definition on the properties of $\{x_{cl_i}\}$ will be made shortly. We set $x_i = x_{cl_i} + \partial x_i$ with x_{cl_i} being independent of x_i, for $1 \leqslant i < N$. From this point forward, let us set $\partial t_i = \partial t = \Delta t/N$. We may apply this substitution to the path integral in (13), but, for the moment, let us focus on the action:

$$\begin{aligned} S = &\sum_{i=2}^{N} \left(\frac{m(x_{cl_i} - x_{cl_{i-1}} + \partial x_i - \partial x_{i-1})^2}{2\partial t^2} - V(x_{cl_i} + \partial x_i) \right) \partial t \\ &+ \left(\frac{m(x_{cl_1} - x_0 + \partial x_1)^2}{2\partial t^2} - V(x_{cl_1} + \partial x_1) \right) \partial t. \end{aligned} \tag{15}$$

We assume $\{\partial x_i\}$ are small and use a Taylor's series expansion of V to organize S in powers of ∂x_i.

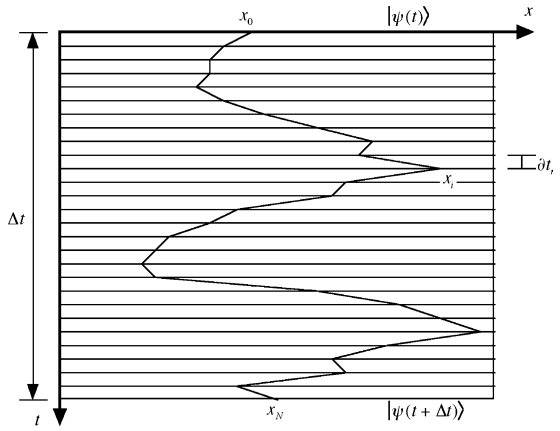

Fig. 1. An arbitrary path from x_0 to x_N. Paths like this one link contributions from $|\psi(t)\rangle$ to $|\psi(t+\Delta t)\rangle$ with a phase difference determined by the action on this path.

$$S = \partial t \sum_{i=2}^{N} \begin{pmatrix} \frac{m(x_{cl_i} - x_{cl_{i-1}})^2}{2\partial t^2} - V(x_{cl_i}) \\ + \frac{m(x_{cl_i} - x_{cl_{i-1}})(\partial x_i - \partial x_{i-1})}{\partial t^2} - \frac{\partial V}{\partial x}\Big|_{x_{cl_i}} \partial x_i \\ + \frac{m(\partial x_i - \partial x_{i-1})^2}{2\partial t^2} - \frac{\partial^2 V}{\partial x^2}\Big|_{x_{cl_i}} \frac{\partial x_i^2}{2} \\ - \frac{\partial^3 V}{\partial x^3}\Big|_{x_{cl_i}} \frac{\partial x_i^3}{3!} + \cdots \end{pmatrix} + \partial t \begin{pmatrix} \frac{m(x_{cl_1} - x_0)^2}{2\partial t^2} - V(x_{cl_1}) \\ + \frac{m(x_{cl_1} - x_{cl_{i-1}})\partial x_1}{\partial t^2} - \frac{\partial V}{\partial x}\Big|_{x_{cl_1}} \partial x_1 \\ + \frac{m\partial x_1^2}{2\partial t^2} - \frac{\partial^2 V}{\partial x^2}\Big|_{x_{cl_1}} \frac{\partial x_1^2}{2} \\ - \frac{\partial^3 V}{\partial x^3}\Big|_{x_{cl_1}} \frac{\partial x_1^3}{3!} + \cdots \end{pmatrix}. \tag{16}$$

Note that the kinetic energy component only contributes to the lowest three orders.

Let us consider with the terms that are first order in ∂x_i. We now finish the definition of $\{x_{cl_i}\}$: we define that these values are such that the first order terms in this sum are zero. Since the ∂x_i are independent of each other, their coefficients must each be zero for this condition to be true. Collecting terms in ∂x_i, for $1 < i < N$, implies that

$$-\frac{m(x_{cl_{i+1}} - x_{cl_i})}{\partial t^2} + \frac{m(x_{cl_i} - x_{cl_{i-1}})}{\partial t^2} - \frac{\partial V}{\partial x}\Big|_{x_{cl_i}} = 0. \tag{17}$$

Arranging the terms into a more familiar form, we have

$$-\frac{\partial V}{\partial x}\Big|_{x_{cl_i}} = m\frac{\frac{(x_{cl_{i+1}} - x_{cl_i})}{\partial t} - \frac{(x_{cl_i} - x_{cl_{i-1}})}{\partial t}}{\partial t}, \tag{18}$$

and we recognize that this is the time-centered discrete form of $F = ma$. Also note that the time-discrete velocity expressions are time-centered at half steps relative to the time centering of the position variables. This prescription is consistent with the leap-frog method used to numerically trace *classical* paths. Hence, we recognize that the path described by $\{x_{cl_i}\}$ is a classical path, justifying its label, *cl*. Also, it becomes reasonable to name the particles that follow these paths *virtual classical particles*.

Fig. 2 depicts a classical path accompanied by its associated variations. It is the contributions of a multitude of these classical paths, at a variety of positions and momenta, that construct the final wavefunction from the initial wavefunction. Also, we make the following distinction: We name ∂t *the classical time step*

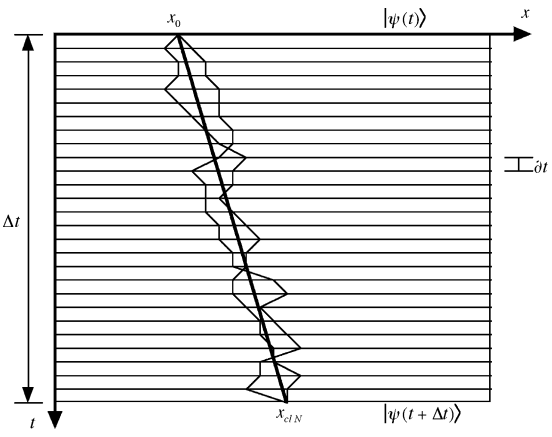

Fig. 2. A classical path is shown, accompanied by variations on that path. The virtual classical particles follow these classical paths, linking quantum wavefunctions from one time to the next while providing a mechanism for the wavefunction to interact with its environment.

because it is the time that separates steps of the classical path, but Δt is *the quantum time step* because it is the interval between evaluations of quantum wavefunctions.

2.4. Initial position and final momentum

We need to consider how to connect the ends of these classical paths to the initial and final wavefunctions. Using the criterion for the term first order in ∂x_1, we have an initial constraint:

$$-\left.\frac{\partial V}{\partial x}\right|_{x_{cl_1}} = m\frac{\frac{(x_{cl_2}-x_{cl_1})}{\partial t} - \frac{(x_{cl_1}-x_0)}{\partial t}}{\partial t}. \tag{19}$$

This equation links the classical path to the integral over x_0.

Now we consider the final constraint. Let us insert $\mathbf{1} = \int \mathrm{d}p_f |p_f\rangle\langle p_f|$ before the $|x_N\rangle$ in (13), resulting in

$$|\psi_f\rangle = \int \mathrm{d}p_f \prod_{j=1}^{N} \mathrm{d}x_j \, |p_f\rangle \left(\frac{\mathrm{i}m}{h\partial t}\right)^{N/2} \frac{1}{\sqrt{h}} \exp\left(-\frac{\mathrm{i}x_N p_f}{\hbar}\right) \exp\left(\frac{\mathrm{i}}{\hbar}S\right) \langle x_0|\psi_0\rangle. \tag{20}$$

Performing the above substitution and requiring that the coefficient of the ∂x_N be zero implies the following constraint:

$$-\frac{P_f}{\partial t} + \frac{m(x_{cl_N} - x_{cl_{N-1}})}{\partial t^2} - \left.\frac{\partial V}{\partial x}\right|_{x_{cl_N}} = 0. \tag{21}$$

Rearranging gives

$$-\left.\frac{\partial V}{\partial x}\right|_{x_{cl_N}} = \frac{P_f - \frac{m(x_{cl_N}-x_{cl_{N-1}})}{\partial t}}{\partial t}. \tag{22}$$

(18) gives $N-2$ constraints on $\{x_{cl_i}\}$, and (19) and (22) provide the $(N-1)$th and Nth constraint, allowing $\{x_{cl_i}\}$ to be uniquely identified by x_0 and P_f.

Rewriting $|\psi_f\rangle$,

$$|\psi_f\rangle = \int \mathrm{d}p_f \int \mathrm{d}x_0 \, |p_f\rangle \frac{1}{\sqrt{h}} \exp\left(-\frac{\mathrm{i}x_{cl_N}p_f}{\hbar}\right) \exp\left(\frac{\mathrm{i}}{\hbar}S_{cl}\right) A\langle x_0|\psi_0\rangle, \tag{23}$$

where

$$S_{cl} \equiv \partial t \sum_{i=1}^{N} \left(\frac{m(x_{cl_i} - x_{cl_{i-1}})^2}{2\partial t^2} - V(x_{cl_i})\right) \tag{24}$$

(using $x_{cl_0} \equiv x_0$), the zeroth order terms of the action,

$$A = \int \prod_{i=1}^{N} \mathrm{d}(\partial x_i) \left(\frac{\mathrm{i}m}{h\partial t}\right)^{N/2} \exp\left(\frac{\mathrm{i}}{\hbar}S_2\right), \tag{25}$$

an N-dimensional integral, and

$$S_2 = \partial t \sum_{i=2}^{N} \begin{pmatrix} \frac{m(\partial x_i - \partial x_{i-1})^2}{2\partial t^2} - \left.\frac{\partial^2 V}{\partial x^2}\right|_{x_{cl_i}} \frac{\partial x_i^2}{2} \\ -\left.\frac{\partial^3 V}{\partial x^3}\right|_{x_{cl_i}} \frac{\partial x_i^3}{3!} + \cdots \end{pmatrix} + \partial t \begin{pmatrix} \frac{m\partial x_1^2}{2\partial t^2} - \left.\frac{\partial^2 V}{\partial x^2}\right|_{x_{cl_1}} \frac{\partial x_1^2}{2} \\ -\left.\frac{\partial^3 V}{\partial x^3}\right|_{x_{cl_1}} \frac{\partial x_1^3}{3!} + \cdots \end{pmatrix}, \tag{26}$$

the second order terms and higher of the action. A substitution, $p_f = p_{cl_f}(p_0)$ (using $p_0 \equiv m\frac{x_{cl_1}-x_0}{\partial t}$), can be used to identify these paths using initial conditions only.

2.5. The matrix

(This section largely follows Chapter 14 of [20], with significant points of customization.) Consider S_2. Let us assume that the terms higher than second order in ∂x_i are neglectable. This allows us to write S_2 in the following form:

$$S_2 = \frac{m}{2\partial t}\eta^j M^i_j \eta_i, \tag{27}$$

using the Einstein summation convention, where $\eta \equiv (\partial x_1, \partial x_2, \ldots, \partial x_N)^{\mathrm{T}}$, M is a tridiagonal $N \times N$ matrix,

$$M = u - w = \begin{pmatrix} 2 & -1 & 0 & \cdots & \cdots & 0 \\ -1 & 2 & -1 & & & \\ 0 & -1 & 2 & \ddots & & \\ \vdots & & \ddots & \ddots & \ddots & 0 \\ \vdots & & & \ddots & 2 & -1 \\ 0 & \cdots & \cdots & 0 & -1 & 1 \end{pmatrix} - \begin{pmatrix} w_1 & 0 & \ldots & 0 \\ 0 & w_2 & & \vdots \\ \vdots & & \ddots & 0 \\ 0 & \cdots & 0 & w_N \end{pmatrix} \tag{28}$$

and

$$w_i \equiv \frac{\partial t^2}{2m}\frac{\partial^2 V}{\partial x^2}\bigg|_{x_{cl_i}}. \tag{29}$$

For any matrix M, there exists a unitary transformation U so that $M' = UMU^{-1}$ is diagonal. The basis set of M' maps to the eigenvectors of M. In the new basis set, $\eta' = U\eta = (\partial x'_1, \partial x'_2, \ldots, \partial x'_N)$ and M' is diagonal:

$$M' = \begin{pmatrix} m_1 & 0 & \cdots & 0 \\ 0 & m_2 & & \vdots \\ \vdots & & \ddots & 0 \\ 0 & \cdots & 0 & m_N \end{pmatrix}, \tag{30}$$

where $\{m_i\}$ are the eigenvalues of M (and M'). Therefore S_2 may be rewritten as

$$S_2 = \frac{m}{2\partial t}\eta'^j M'^i_j \eta'_i = \frac{m}{2\partial t}\sum_{i=1}^{N} \partial x_i'^2 m_i. \tag{31}$$

This makes A separable:

$$A = \int \prod_{j=1}^{N} \mathrm{d}(\partial x'_j)\left(\frac{\mathrm{im}}{\hbar\partial t}\right)^{N/2} \exp\left(\frac{\mathrm{i}}{\hbar}\frac{m}{2\partial t}\sum_{i=1}^{N}\partial x_i'^2 m_i\right) = \left(\frac{\mathrm{im}}{\hbar\partial t}\right)^{N/2}\prod_{i=1}^{N}\int \mathrm{d}(\partial x'_j)\exp\left(\frac{\mathrm{im}}{2\hbar\partial t}m_{\mathrm{i}}\partial x_i'^2\right). \tag{32}$$

The integrals are Gaussian, so A simplifies

$$A = \left(\frac{\mathrm{im}}{h\partial t}\right)^{N/2} \prod_{i=1}^{N} \sqrt{\frac{2\pi\hbar\partial t}{\mathrm{im}\cdot m_i}} = \left(\frac{\mathrm{im}}{h\partial t}\right)^{N/2} \left(\frac{h\partial t}{\mathrm{im}}\right)^{N/2} \frac{1}{\sqrt{\prod_{i=1}^{N} m_i}} = \frac{1}{\sqrt{\det(M')}} \tag{33}$$

because the determinant of a diagonal matrix is the product of its elements. But since $\det(M') = \det(UMU^{-1}) = \det(U)\det(M)\det(U^{-1}) = \det(M)$,

$$A = \frac{1}{\sqrt{\det(M)}}. \tag{34}$$

(There are issues concerning when this determinant goes to zero, but that will be addressed in the next section.)

Then $|\psi_f\rangle$ becomes

$$|\psi_f\rangle = \int \mathrm{d}p_f \int \mathrm{d}x_0 \, |p_f\rangle \frac{1}{\sqrt{h\det(M)}} \exp\left(-\frac{\mathrm{i}x_{cl_N}p_f}{\hbar}\right) \exp\left(\frac{\mathrm{i}}{\hbar}S_{cl}\right) \langle x_0|\psi_0\rangle \tag{35}$$

a two-dimensional integral, with M defined above.

2.6. The determinant

At this point, this discussion substantially diverges from Schulman's [20] and, to the authors' knowledge, is not expressed elsewhere. Let us take a closer look at evaluating the determinant of the above matrix. At first glance, it appears calculating this determinant may be necessary to allocate at least O(N) storage, but an alternative approach was developed to reduce the storage to O(1). This approach was developed to find a convenient form to calculate it numerically, but it also shows the likelihood of it causing the determinant to become singular, which is the results from the "conjugate points" and "caustics" studied at length in other references [13,16,20–22,49].

Let us consider the determinant of an $i \times i$ upper-left minor of M and call it d_i. For $2 < i < N$,

$$d_i = \begin{vmatrix} 2-w_1 & -1 & 0 & \cdots & \cdots & 0 \\ -1 & 2-w_2 & -1 & & & \\ 0 & -1 & 2-w_3 & \ddots & & \\ \vdots & & \ddots & \ddots & \ddots & 0 \\ \vdots & & & \ddots & 2-w_{i-1} & -1 \\ 0 & \cdots & \cdots & 0 & -1 & 2-w_i \end{vmatrix}. \tag{36}$$

Evaluating this determinant by minors gives

$$d_i = (2-w_i) \begin{vmatrix} 2-w_1 & -1 & 0 & \cdots & 0 \\ -1 & 2-w_2 & -1 & & \vdots \\ 0 & -1 & \ddots & \ddots & 0 \\ \vdots & & \ddots & 2-w_{i-2} & -1 \\ 0 & \cdots & 0 & -1 & 2-w_{i-1} \end{vmatrix} - (-1) \begin{vmatrix} 2-w_1 & -1 & 0 & \cdots & 0 \\ -1 & 2-w_2 & \ddots & & \vdots \\ 0 & \ddots & \ddots & \ddots & 0 \\ \vdots & & \ddots & 2-w_{i-2} & 0 \\ 0 & \cdots & 0 & 0 & -1 \end{vmatrix}. \tag{37}$$

But we may recognize that the first determinant is d_{i-1} and the second becomes $(-1)d_{i-2}$. Therefore,

$$d_i = (2-w_i)d_{i-1} - d_{i-2}. \tag{38}$$

There are a few special cases: For d_N, d_1, and d_2,

$$d_N = (1 - w_i)d_{N-1} - d_{N-2}, \tag{39}$$
$$d_1 = (2 - w_1), \tag{40}$$
$$d_2 = (2 - w_2)d_1 - 1, \tag{41}$$

or (38) may be used to calculate d_2 and d_1 if we define

$$d_0 \equiv 1 \tag{42}$$

and

$$d_{-1} \equiv 0. \tag{43}$$

The above expressions provide a complete description, in the form of an iterative method, for evaluating the determinant of M. Algorithmically, this evaluation can be performed alongside the evaluation of the classical path using (18) with a minimum of storage space, because w_i is only a function of x_{cl_i}.

Rearranging (38) gives

$$(d_i - 2d_{i-1} + d_{i-2}) + w_i d_{i-1} = 0. \tag{44}$$

We recognize that this is a time-discrete leap-frog-method form of the following ordinary differential equation:

$$\frac{\mathrm{d}^2 y(t)}{\mathrm{d}t^2} + w(t)y(t) = 0, \tag{45}$$

which is the simple harmonic oscillator equation with a time-dependent frequency term, where $y(t) = d_t$ and $w(t) = w_{t+1} = \frac{\partial t^2}{2m}\frac{\partial^2 V}{\partial x^2}\Big|_{x_{cl_{i+1}}}$. Interpreting (40) and (41) in this context implies the following initial conditions on y:

$$y(0) \equiv 1, \tag{46}$$
$$\dot{y}(0) \equiv 1 - w_1. \tag{47}$$

The determinant is given by $y(N) - y(N-1)$.

Let us investigate the likelihood of d_N becoming zero. For the sake of argument, let us make w constant. If $w = 0$, then y begins at 1 and increases linearly without bound, resulting in a determinant of 1. If $w < 0$, which corresponds to a defocusing V, then y will increase without bound exponentially, resulting in a determinant greater than 1.

However, if $w > 0$, corresponding to a V that focuses, then y will behave as a sine wave with a period of

$$T = \frac{2\pi}{\sqrt{w}}. \tag{48}$$

Because the initial conditions are non-zero with a positive slope and w is typically less than 1, $\dot{y}$ will not become zero within one-eighth period. Therefore, if we wish to be sure of never encountering a path whose determinant becomes zero, then

$$N < \frac{\pi}{4\sqrt{w}} = \frac{\pi}{4\partial t}\sqrt{2m\Big/\frac{\partial^2 V}{\partial x^2}}, \tag{49}$$

but ∂t is related to N, so the requirement becomes

$$\Delta t < \frac{\pi}{4}\sqrt{2m\Big/\frac{\partial^2 V}{\partial x^2}}. \tag{50}$$

Here we have a recommended upper bound on Δt, the time between quantum wavefunction evaluations, depending on the physics of the system. This is a worst case scenario, when V has a period of sustained focusing (e.g., in the simple harmonic oscillator). To the authors' knowledge, this prediction (50) is not made and utilized elsewhere.

For typical physical parameters, however, other issues, such as changes in the effective V due to the movement of other particles, will require a Δt significantly smaller than required by (50). In practice, the period is long enough (or $\frac{\partial^2 V}{\partial x^2}$ is small enough) so that d_N, at worst, remains within 1% of 1.

2.7. Summary

We now have a method to time-evolve quantum wavefunctions using classical calculations designed for computation. Here we gather the equations in preparation for implementation. We calculate the following double integral:

$$|\psi(t+\Delta t)\rangle = \int \mathrm{d}p_0 \int \mathrm{d}x_0\, |p_{cl_f}\rangle \left(\frac{\partial p_{cl_f}}{\partial p_0}\right) \frac{1}{\sqrt{h\det(M)}} \exp\left(-\frac{\mathrm{i}x_{cl_N}p_{cl_f}}{\hbar}\right) \exp\left(\frac{\mathrm{i}}{\hbar}S_{cl}\right) \langle x_0|\psi(t)\rangle. \tag{51}$$

A large number of classical paths, each uniquely identified by the dummy variables x_0 and $p_0 \equiv m\frac{x_{cl_1}-x_0}{\partial t}$, are traced using

$$-\left.\frac{\partial V}{\partial x}\right|_{x_{cl_i}} = m\frac{\frac{(x_{cl_{i+1}}-x_{cl_i})}{\partial t} - \frac{(x_{cl_i}-x_{cl_{i-1}})}{\partial t}}{\partial t} \tag{18}$$

over $N = \Delta t/\partial t$ time steps (using $x_{cl_0} \equiv x_0$). The action along each path, S_{cl}, is given by

$$S_{cl} \equiv \partial t \sum_{i=1}^{N} \left(\frac{m(x_{cl_i} - x_{cl_{i-1}})^2}{2\partial t^2} - V(x_{cl_i})\right). \tag{24}$$

Simultaneous with the evaluation of each classical path, $\det(M)$ is calculated using an iterative method:

$$d_i = (2 - w_i)d_{i-1} - d_{i-2}, \tag{38}$$

for $1 \leqslant i < N$, using initial conditions

$$d_0 \equiv 1 \quad \text{and} \quad d_{-1} \equiv 0, \tag{42 \& 43}$$

where

$$w_i \equiv \frac{\partial t^2}{2m}\left.\frac{\partial^2 V}{\partial x^2}\right|_{x_{cl_i}}. \tag{29}$$

The determinant itself is

$$\det(M) = (1 - w_N)d_{N-1} - d_{N-2}. \tag{52}$$

Finally, the final classical momentum, p_{cl_f}, is given by

$$-\left.\frac{\partial V}{\partial x}\right|_{x_{cl_N}} = \frac{p_{cl_f} - \frac{m(x_{cl_N}-x_{cl_{N-1}})}{\partial t}}{\partial t}. \tag{53}$$

This completes the time evolution of $|\psi\rangle$.

3. Implementation

3.1. Numbers

We now need to focus on implementing the methods described in the last section to a numerical technique appropriate for current computer hardware. This section defines and details the organization of these semiclassical calculations to evolve quantum wavefunctions. The following presentation introduces methods and results that are new and have not been located in any previous publication.

The total wavefunction is assumed to be separable into wavefunctions for each particle:

$$|\Psi\rangle = \prod_l |\psi_l\rangle \tag{54}$$

which is also known as the ''mean-field'' approximation. This representation neglects quantum statistics and correlation effects, but it is sufficient at this stage because our focus in this article is on the methods described the previous section. We represent each wavefunction on a set of grid points in space, thus discretizing the wavefunctions. Each $\psi_l(x) \equiv \langle x|\psi_l\rangle$ is a complex number. All wavefunctions are begun with a complete description of their initial state at $t = 0$. At any time t, the information contained in all the $\psi_l(x)$'s *alone* is used to update the wavefunctions to the next Δt.

(51) contains a prescription for organizing the classical paths. The obvious solution is to approximate the integral over x_0 with a sum, and assign values of x_0 to the grid points used to represent $\psi_l(x)$. However, what is missing is how to link these paths to the grid point representation of the final wavefunction. Clearly defining this link is very important for the correct evolution of these discretized wavefunctions. We show this link by hitting a $\langle x_f|$ bra on both sides of the equation. (51) becomes

$$\langle x_f|\psi(t+\Delta t)\rangle = \sum_{p_0}\sum_{x_0} \exp\left(\frac{\mathrm{i}x_f p_{cl_f}}{\hbar}\right) \exp\left(-\frac{\mathrm{i}x_{cl_N} p_{cl_f}}{\hbar}\right) \frac{\exp(\mathrm{i}S_{cl}/\hbar)}{h\sqrt{\det(M)}} \langle x_0|\psi(t)\rangle \Delta x \Delta p. \tag{55}$$

We assume the majority of the effects on this value will be due to phase variations between classical paths, expressed in S_{cl}, therefore we assume $\left(\frac{\partial p_{cl_f}}{\partial p_0}\right)$ varies negligibly from 1. Each $\psi_l(x_f, t + \Delta t)$ acquires the value of a double sum. Note that the classical paths can weave, and end, in between grid points and *at the same time* (55) provides a means to link the initial and final wavefunctions on the same set of grid points. This feature is not provided in other theoretical studies of the semiclassical method.

One other issue to examine is the range of momenta. The paths of the original path integral essentially explore all of phase space. The conversion to classical paths allows us to ''strategically poll'' phase space, but the sampling needs to be just as thorough. We have established that x_0 will range over all grid points, which is the entire space of the calculation, so it seems reasonable to say that p_0 will range over all momenta of the calculation. What is the range of possible momenta of this calculation? The Nyquist theorem states that a maximum frequency can be represented on a series of grid points in time. This theorem has a simple extension to the greatest momenta that can be represented using grid points in space.

$$p_{\max} = h/2\Delta x, \tag{56}$$

where Δx is the grid spacing and h is Planck's constant. Since the representation is complex, negative momenta are allowed, so the range of p_0 is $-p_{\max} < p_0 < p_{\max}$. The resolution of the momentum representation of the wavefunction, $\psi_l(p)$, is the same as that of the position representation. Since we justified the spatial resolution using $\psi_l(x)$, it seems reasonable that the resolution of the p_0 distribution should be at least that of $\psi_l(p)$. Although this is not a formal argument, the success of this momentum distribution has been seen empirically.

3.2. Simulations

We applied the above algorithm to a variety of physical scenarios, testing both the validity of the above theoretical approach and the robustness of the one-dimensional implemenation. To help establish the method's relevance to quantum phenomena, the earliest test cases focused on well-known examples of quantum mechanics.

Our earliest quantitative analyses of the quantum PIC code's fidelity to quantum mechanics was performed using a Gaussian wavefunction in free space, the simple harmonic oscillator, and the infinite square well.

The eigenstates infinite square well are known [52] to be

$$\psi_n(x) \propto \sin\left(\frac{\pi n x}{L}\right) \tag{57}$$

with corresponding energy eigenstates:

$$E_n = \frac{\hbar^2 \pi^2 n^2}{2mL^2}, \tag{58}$$

where m is the mass of the particle, L is the width of the well, and n is a positive integer. The simple harmonic oscillator has an external potential:

$$V(x) = \frac{1}{2} m\omega^2 x^2, \tag{59}$$

where ω is the potential's natural angular frequency of oscillation. This leads to the eigenstates:

$$\psi_n(x) \propto \exp\left(-\frac{m\omega x^2}{2\hbar}\right) H_n\left(x\sqrt{2m\omega/\hbar}\right), \tag{60}$$

where H_n are the Hermite polynomials, with a regularly spaced energy spectrum:

$$E_n = \hbar\omega(n + 1/2), \tag{61}$$

where n is a nonnegative integer. The time evolution of these eigenstates are described solely by an overall phase changing at a monotonic rate proportional to the energy eigenvalue of their state:

$$\psi_n(x,t) = \psi_n(x,0) \exp\left(-\frac{\mathrm{i}E_n t}{\hbar}\right). \tag{62}$$

To the level that the numerics allow, we were able to model the eigenstates of both the infinite square well and simple harmonic oscillator, including their time evolution. We were also able to model and measure superpositions of these eigenstates, both generated as explicit superpositions and as arbitrarily selected wavefunctions. Fig. 3 shows eigenstates evolving in an infinite square well, while Fig. 4 shows wavefunctions interacting with a simple harmonic oscillator potential.

For the infinite square well, the initial conditions of different runs were set to the theoretical eigenstates of the system. At all times, the spatial extent of the states remained as constant, as we could expect. Direct measurement of the phase at later time steps matched the prediction of (62) and (58) within the time step resolution after arbitrarily large time step counts. A comparison is shown in Table 1.

Our models using the simple harmonic oscillator system gave a similar degree of consistency with theory. Fig. 4 shows a run using an arbitrary superposition of the $n = 0$, $n = 1$, $n = 5$, and $n = 7$ states. The simulation preserved the superposition of these states sufficient to extract their energies from a code output. The quality of the energy spectrum increased proportionally to the number of time steps, as we would expect from increasing the temporal resolution of the data. The data also revealed little

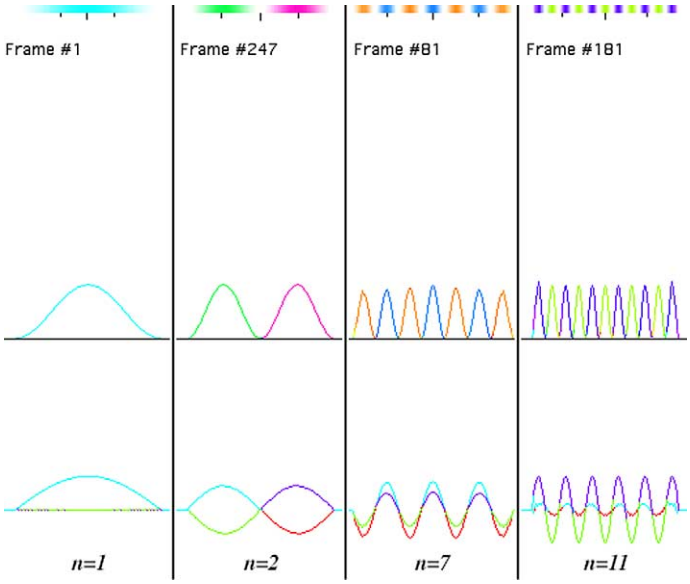

Fig. 3. Example eigenstates of the infinite square well. Frames from runs initialized with the $n = 1, 2, 7$, and 11 eigenstates are shown, demonstrating fidelity to theoretical predictions of these eigenstates.

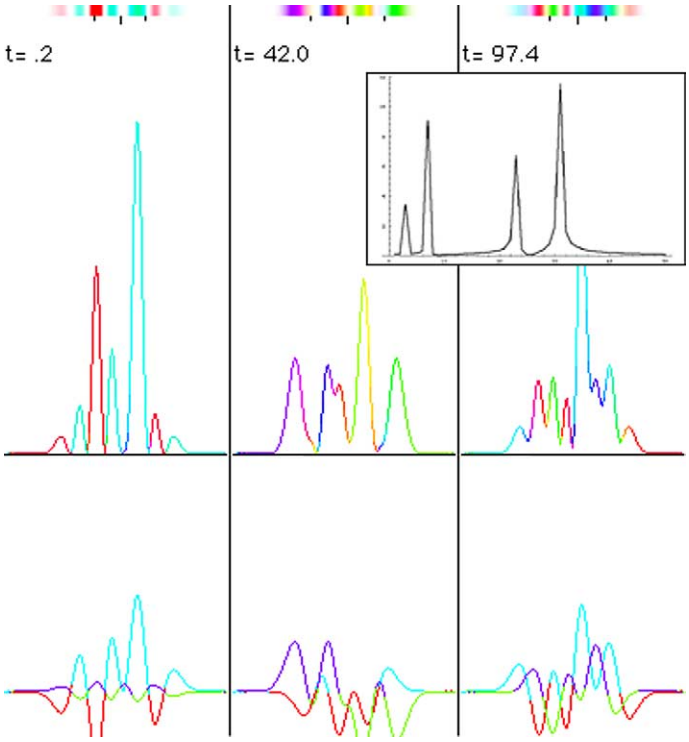

Fig. 4. A simulation of an arbitrary superposition of the $n = 0, 1, 5$, and 7 eigenstates of the simple harmonic oscillator. The measured energy spectrum of the system is inset. The positions of the maxima in this energy spectrum agree with that predicted by theory.

Table 1
Comparison of theory and simulation predictions of the oscillation period for various eigenstates of the infinite square well depicted in Fig. 3 ($h = 64$, $m = 1$, $\Delta t = 0.2$, $L = 120$)

State $\|n\rangle$	Theory (*Period*)	Simulation (*Period*)
$n = 1$	1800	1798 ± 3
$n = 2$	450	449.6 ± 1.6
$n = 7$	36.7	36.8 ± 0.4
$n = 11$	14.88	14.8 ± 0.4

The unit of time is arbitrary.

Table 2
Comparison of theory and simulation for the run of a superposition of simple harmonic oscillator eigenstates depicted in Fig. 4, indicating significant corroboration between our code and quantum mechanics ($h = 64$, $m = 1$, $\Delta t = 0.2$, $\omega = 1/8$)

SHO state $\|n\rangle$	Theory (*Energy*/$\hbar\omega$)	Simulation (*Energy*/$\hbar\omega$)
$n = 0$	0.5	0.50 ± 0.02
$n = 1$	1.5	1.49 ± 0.02
$n = 5$	5.5	5.48 ± 0.06
$n = 7$	7.5	7.48 ± 0.06

significant evidence of error such as crosstalk, harmonic distortion, or noise, providing reinforcing evidence of its fidelity to quantum mechanics. The energy values of the peaks measured in the spectrum were consistent, within the resolution of the spectrum, with the eigenvalues predicted by (61) given the initial conditions. Table 2 compares the theoretical predictions of the energy peaks with those extracted from the simulation.

Our free-space modeling focused on the evolution of a wavefunction whose initial state was a simple Gaussian. Quantum theory predicts that such a system will evolve and expand naturally, as described in [52], with the width:

$$\Delta x = \frac{a}{\sqrt{2}}\sqrt{1 + \frac{\hbar^2 t^2}{m^2 a^4}} \tag{63}$$

as a function of time t. The evolution of this problem is depicted in Fig. 5.

We discovered that precise modeling of the free-space expansion of a Gaussian wavefunction was surprisingly good at revealing subtle errors in our algorithm and implementation. This test case guided much of our model's evolution towards greater physical accuracy. The final incarnation of our code generated a simulation that coincided with the analytical solution within the expected roundoff error of the computation due to single-precision floating-point. A comparison of a Gaussian's expansion with the theoretical prediction (62) is shown in Fig. 6.

3.3. Barrier tunnelling

Our simulations of barrier tunnelling duplicated all qualitative characteristics known in the problem, most especially the energy-dependent partial transmission of the wavefunction when transmission would not have been allowed classically. We studied the interaction between a wavefunction and a barrier ideally expressed as a potential at a constant height V_0 in a region of width a while being zero elsewhere. An example of our model of this interaction is shown in Fig. 7. Previous analyses of barrier tunnelling using semiclassical methods [53,54] utilize the Van Vleck–Gutzwiller–Maslov form of the semiclassical propagator on

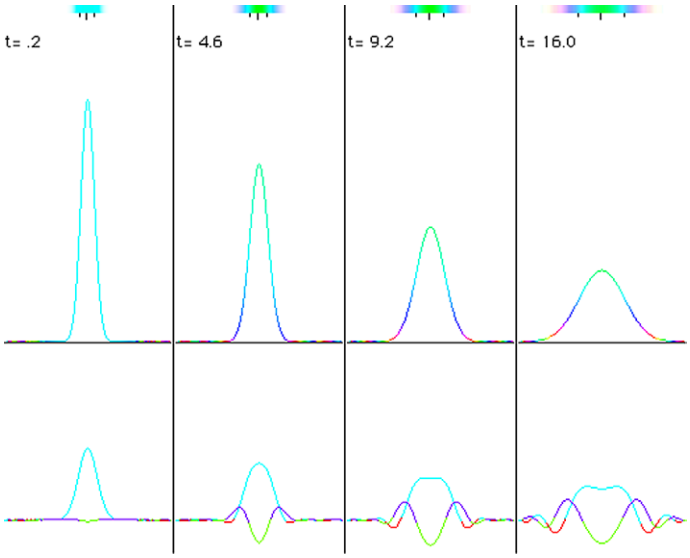

Fig. 5. Four frames of the evolution of a stationary Gaussian in free space.

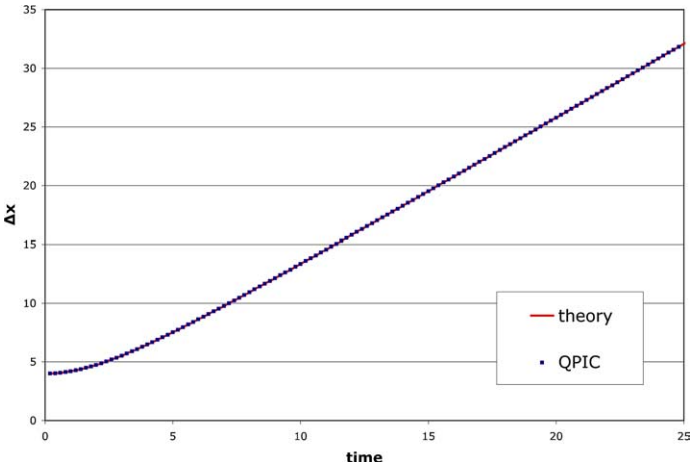

Fig. 6. Comparison of theory (line) and simulation (squares) for the width (Δx) of a Gaussian wavefunction expanding in free space as a function of time. The initial Δx of the Gaussian was four grids, and the simulation was stopped when the wavefunction began to interact with the edge of simulation space. Neighboring squares are one time step apart, and their size approximates the error expected due to single-precision ($h = 64$, $m = 1$, $\Delta t = 0.2$). The QPIC code provided excellent agreement with quantum theory.

a set of classical paths linking points over arbitrarily long time intervals. The study shown here utilizes paths, each spanning short time intervals, to connect one quantum wavefunction to the reconstructed one at the next quantum time step.

The potential used for this calculation approximates the potential barrier of the well-known theoretical case of quantum tunnelling. Rather than allow discontinuities in the potential and infinite forces at the barrier edges, the computational simulation used steeply sloped edges on its potential barrier. This model results in forces compatible with the numerics. Consequently, the exact shape of the barrier in the

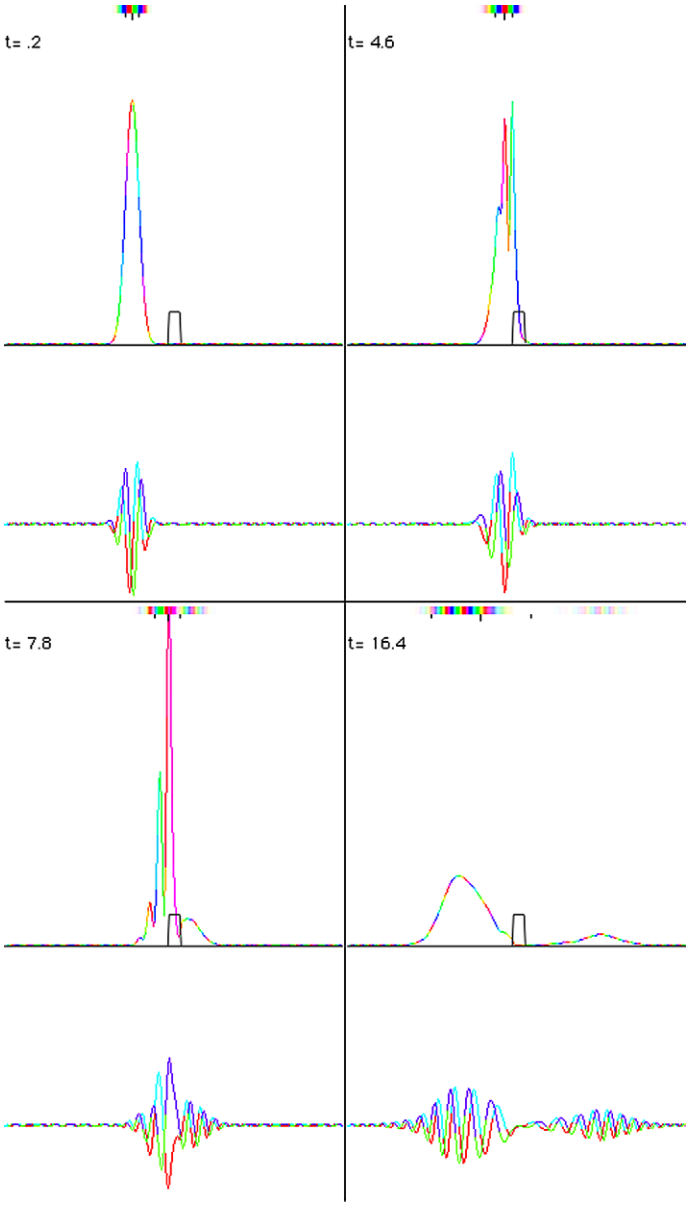

Fig. 7. Evolution of a Gaussian wavefunction colliding with a square barrier eight grids wide in the center (small rectangle). The energy of the Gaussian is just enough for a significant amount of transmission and reflection, seen in the last frame.

computation is unresolved simply because its edges have features smaller than the grid spacing. Because of the discrepancies between the theoretical and computational versions of the quantum barrier problem, quantitative comparison becomes challenging to produce. Derived from [52], the transmission probability of a Gaussian with an initial width σ and initial average momentum $\hbar k_0$ through a potential barrier of width a and height V_0 is

$$T(\sigma) = \frac{2\sigma}{\sqrt{2\pi}} \int_{-\infty}^{\infty} \exp(-2\sigma^2(k-k_0)^2) \frac{1}{1 + \left(\frac{mV_0/\hbar^2}{kq}\right) \sin h^2(qa)} \mathrm{d}k, \tag{64}$$

where

$$q \equiv \sqrt{2mV_0/\hbar^2 - k^2}. \tag{65}$$

We were able to produce a comparison of (63) and (64) with the code output in Fig. 8.

Fig. 8 shows the probability of transmission through a potential barrier for a quantum wavefunction whose initial state is a Gaussian moving towards that barrier. The horizontal axis sets the initial width of the wavefunction, and each group of curves corresponds to a different barrier height. The quantum PIC code inherited its spatial resolution, the grid spacing, from the plasma PIC code. Theory predicts that the transmission probability can vary rapidly as a function of barrier width (by as much as 30% for one grid-spacing change in width). Bearing that and the limited resolution of the barrier size in mind, we should expect the quantum PIC code's results to deviate from theory to the extent that the uncertainty in the barrier width results in such deviations in transmission probability. The theoretical predictions plotted in Fig. 8 demonstrate these deviations in transmission probability.

3.4. Beyond textbook quantum mechanics

After establishing its fidelity to quantum mechanics, particularly how single quantum particles interact with its environment, we applied the quantum PIC code to various multiparticle systems. For the one-dimensional code, we focused on electrostatic interactions between wavefunctions represented using the mean-field approximation. We considered multiparticle systems interacting in external potentials that we knew well, such as the infinite square well, as well as potentials not as well established, such as the one-dimensional atom, whose potential is proportional to the absolute distance from its center. Although a

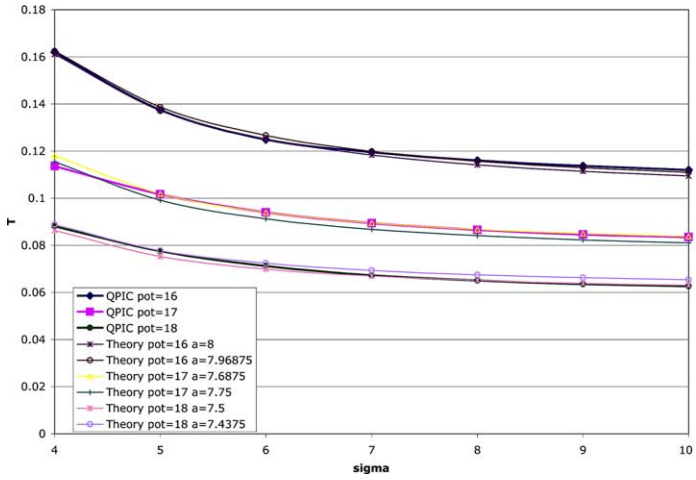

Fig. 8. The transmission probability of a moving Gaussian wavefunction to tunnel through a potential barrier. The thick lines are the results of quantum PIC simulation, while the thin lines are theoretical predictions using (63) and (64) for slightly different barrier widths (a), corresponding to the uncertainty in the dimensions of the potential in the simulation. The three groups of lines correspond to the different barrier heights used (pot), and the horizontal axis is the width (sigma) of the initial Gaussian wavefunction. The vertical axis is the fraction of the wavefunction that is transmitted, and all distances are multiples of the grid spacing, while the units of the other values are arbitrary ($h = 64$, $m = 1$, $k_0 = 1/2$, $\Delta t = 0.1$). These results demonstrate the code's high fidelity to quantum mechanics.

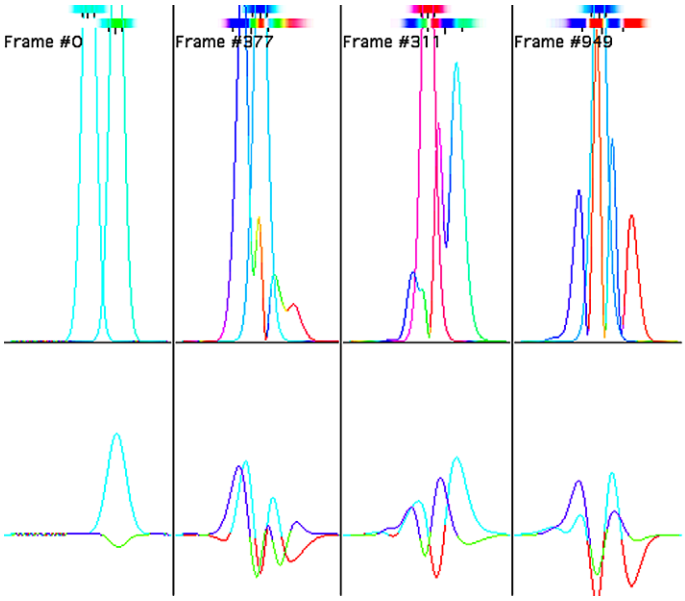

Fig. 9. Four frames of two mutually interacting electrons in a 1D atom potential ($V \propto |x|$). While one electron was centered at with the potential and the other was displaced, the initial state of both electrons were stationary Gaussian wavefunctions. Post-processing of the data from this simulation led to interesting insights into this physical system.

detailed analysis of these systems are outside the scope of this article, we can present a system with two-electrons in a one-dimensional atom in Fig. 9.

Although a detailed presentation of this analysis is reserved for a future article, we applied the quantum PIC code to systems about which we knew little, and we were able to extract high-quality predictions from their time evolution not easily addressed using theory. In a future article, we will explore this example of how the quantum PIC code can be applied as a tool to further our understanding of nontrivial quantum systems.

4. Conclusion

We have successfully created, implemented, and tested an alternative method to model the dynamic evolution of quantum-mechanical wavefunctions. This method is based on the semiclassical approximation of Feynman path integrals, allowing the computation to be simplified to the tracing of many classical paths. This prescription provides a way to utilize plasma PIC implementations designed for parallel computers for modeling of quantum mechanics. Within the known limits of the numerics, our one-dimensional implementation of this technique has successfully duplicated all well-established quantum phenomena. This article lays the foundation for the application of the semiclassical method to simulations of time-dependent, interacting quantum wavefunctions.

Although the implementation discussed above is one-dimensional, the technique is also being applied in a two-dimensional implementation. Given the phase-space sampling described in Section 3.1, the pessimistic scaling estimate for this approach would be $O(N^2)$ for a system with N grid points. So far we are seeing scaling almost as low as $O(N)$ using optimization techniques applicable only to higher dimensions, which gives us some confidence in its utility for real-world problems. The work continues at the

UCLA Plasma Physics group with John Tonge and the authors. Our intention is to incorporate additional code optimizations into the code and extend physics addressed the code possible with two dimensions, such as magnetism and nuclear fusion. We intend to address these topics in a subsequent publication.

Acknowledgments

We wish to thank John M. Dawson for the insight, vision, discussion, and support he gave for this work. His contribution was critical for this project. We greatly appreciate the discussion, feedback, and help of John Tonge. The original development of the method was supported by LLNL ISCR 99-012 and was performed as part of the doctoral dissertation of D. Dauger. Further work has been performed with the support of a grant from NSF.

References

[1] R.B. Gerber, V. Buch, M.A. Ratner, Simplified time-dependent self consistent field approximation for intramolecular dynamics, Chem. Phys. Lett. 91 (1982) 173.
[2] U. Peskin, M. Steinberg, A temperature-dependent Schrödinger equation based on a time-dependent self consistent field approximation, J. Chem. Phys. 109 (1998) 704.
[3] K.M. Christoffel, P. Brumer, Quantum and classical dynamics in the stadium billiard, Phys. Rev. A 33 (1986) 1309.
[4] E.J. Heller, Frozen Gaussians: a very simple semiclassical approximation, J. Chem. Phys. 75 (1981) 2923.
[5] N. Makri, Time-dependent self-consistent field approximation with explicit 2-body correlations, Chem. Phys. Lett. 169 (1990) 541.
[6] L. de Broglie, Recherches sur la théorie des Quanta, Ann. d. Phys. 3 (10) (1925) 22 (Thèses, Paris 1924).
[7] J.H. Van Vleck, The correspondence principle in the statistical interpretation of quantum mechanics, Proc. Natl. Acad. Sci. USA 14 (1928) 178.
[8] Commonly known today as "WKB", the method, as it was originally presented, was designed specifically for solving Schrödinger's equation of wave mechanics. It is in such common use today that citations to the original references are difficult to find. The original three papers are:
G. Wentzel, Eine Verallgemeinerung der Quantenbedingungen für Zwecke der Wellenmechanik, Z. Phys. 38 (1926) 518;
H.A. Kramers, Wellenmechanik und halbzahlige Quantisierung, Z. Phys. 39 (1926) 828;
L. Brillouin, La mècanique ondulatoire de Schrödinger; une mèthode gènèrale de rèsolution par approximations successives, C.R. Acad. Sci. 183 (1926) 24.
[9] E. Schrödinger, Quantiseirung als Eigenwertproblem, Ann. d. Phys. 79 (1926) 361;
E. Schrödinger, Ann. d. Phys. 79 (1926) 489;
E. Schrödinger, Ann. d. Phys. 80 (1926) 437;
E. Schrödinger, Ann. d. Phys. 81 (1926) 109.
[10] P.M. Dirac, Phys. Z. Sowjetunion 3 (1933) 1.
[11] R.P. Feynman, Rev. Mod. Phys. 20 (1948) 367–387.
[12] R.P. Feynman, A.R. Hibbs, Quantum Mechanics and Path Integrals, McGraw-Hill, New York, 1965.
[13] M.C. Gutzwiller, Phase-integral approximation in momentum space and the bound states of an atom, J. Math. Phys. 8 (1967) 1979.
[14] E. Heller, J. Chem. Phys. 94 (1991) 2723.
[15] S. Tomsovic, E. Heller, Phys. Rev. Lett. 67 (6) (1991) 664.
[16] E. Heller, S. Tomsovic, Postmodern quantum mechanics, Phys. Today 46 (7) (1993) 38, and references therein.
[17] S. Tomsovic, E. Heller, Phys. Rev. Lett. 70 (1993) 1405.
[18] S. Tomsovic, E.J. Heller, Long-time semiclassical dynamics of chaos: the stadium billiard, Phys. Rev. E 47 (1993) 282.
[19] V.P. Maslov, M.V. Fedoriuk, Semiclassical Approximations in Quantum Mechanics, Reidel, Dordrecht, 1981 (English translation).
[20] L.S. Schulman, Techniques and Applications of Path Integration, Wiley, New York, 1981, and references therein.
[21] M.A. Sepúlveda, S. Tomsovic, E. Heller, Phys. Rev. Lett. 69 (1992) 402.
[22] M.C. Gutzwiller, Chaos in Classical and Quantum Mechanics, Springer-Verlag, New York, 1990.
[23] O. Buneman, Phys. Rev. 115 (1959) 503.
[24] J.M. Dawson, Princeton University Plasma Physics Laboratory, Project Matterhorn Rept., MATT-4, 1959.

[25] J.M. Dawson, Princeton University Plasma Physics Laboratory, Project Matterhorn Rept., MATT-31, 1960.
[26] J.M. Dawson, Phys. Fluids 5 (1962) 445.
[27] J.M. Dawson, in: Alder, Fernbach, Rotenburg (Eds.), Methods in Computational Physics, vol. 9, Academic Press, New York, 1970, p. 1.
[28] R.W. Hockney, Phys. Fluids 9 (1966) 1826.
[29] J.W. Cooley, J.W. Tukey, Math. Comput. 19 (1965) 297.
[30] J.M. Dawson, C.G. Hsi, R. Shanny, Princeton University Plasma Physics Laboratory, Project Matterhorn Rept., MATT-719, 1969.
[31] J.M. Dawson, Rev. Mod. Phys. 55 (1983) 403.
[32] J.M. Dawson, V.K. Decyk, R.D. Sydora, P. Liewer, High-performance computing and plasma physics, Phys. Today 46 (3) (1993) 64.
[33] V.K. Decyk, Parallel processing of particle simulation models, in: M.F. Heyn, W. Kernbichler (Eds.), Proceedings of the International Workshop on Plasma Physics, Pichl, Austria, February 1992, Current Topics in Astrophysical and Fusion Plasma Research, dbu-[Dbu Graz, Austria, 1992], p. 187.
[34] J.M. Dawson, V.K. Decyk, Particle modeling of plasmas on super-computers, Int. J. Supercomput. Appl. 1 (1987) 24.
[35] J.M. Dawson, The numerical Tokamak: A grand challenge for fusion plasma modeling, in: Proceedings of IAEA Technical Committee Meeting on Advances in Simulation and Modeling Thermonuclear Plasmas, Montreal, Que., Canada, vol. 1, 1992.
[36] J.M. Dawson, Computer modeling of plasma: past, present, future, Phys. Plasmas 2 (1995) 6.
[37] V.K. Decyk, How to write (nearly) portable Fortran programs for parallel computers, Comput. Phys. 7 (1993) 418.
[38] V.K. Decyk, Skeleton PIC Codes for parallel computers, Comput. Phys. Commun. 87 (1995) 87.
[39] V.K. Decyk, D.E. Dauger, P.R. Kokelaar, How to build an AppleSeed: a parallel Macintosh cluster for numerically intensive computing, Phys. Scr. T 84 (2000) 85–88.
[40] M.F. Herman, E. Kluk, H.L. Davis, Comparison of the propagation of semiclassical frozen Gaussian wave functions with quantum propagation for a highly excited anharmonic oscillator, J. Chem. Phys. 84 (1986) 326.
[41] M.S. Child, Semiclassical Mechanics with Molecular Applications, Clarendon Press, Oxford, 1991.
[42] K.G. Kay, Semiclassical propagation for multidimensional systems by an initial value method, J. Chem. Phys. 101 (3) (1994) 2250.
[43] A.R. Walton, D.E. Manolopoulos, A new semiclassical initial value method for Franck-Condon spectra, Mol. Phys. 87 (1996) 961.
[44] X. Sum, H.B. Wang, W.H. Miller, Semiclassical theory of electronically nonadiabatic dynamics: results of a linearized approximation to the initial value representation, J. Chem. Phys. 109 (1998) 7064.
[45] K. Thompson, N. Makri, Rigorous forward–backward semiclassical formation of many-body dynamics, Phys. Rev. E 59 (1999) 4729.
[46] L. Kaplan, E.J. Heller, Overcoming the wall in semiclassical Baker's map, Phys. Rev. Lett. 76 (1996) 1453.
[47] G. Campolieti, P. Brumer, Semiclassical initial value approach for chaotic long-lived dynamics, J. Chem. Phys. 109 (1998) 2999.
[48] N.T. Maitra, E.J. Heller, Semiclassical amplitudes: supercaustics and the whisker map, Phys. Rev. A 61 (1999) 0212107-1.
[49] M. Brack, R.K. Bhaduri, Semiclassical Physics, Addison-Wesley, New York, 1997, and references therein.
[50] E.J. Heller, Proceedings from Les Houchs 1989, in: Chaos and Quantum Physics, North-Holland, Amsterdam, 1989.
[51] F.P. Simotti, E. Vergini, M. Saraceno, Quantitative study of scars in the boundary section of the stadium billiard, Phys. Rev. E 56 (1997) 3859.
[52] J.S. Townsend, A Modern Approach to Quantum Mechanics, McGraw-Hill, New York, 1992.
[53] N.T. Maitra, E.J. Heller, Phys. Rev. Lett. 78 (1997) 3035.
[54] D.H. Zhang, E. Pollak, Phys. Rev. Lett. 93 (2004) 140401.